Multilevel Fast Multipole Algorithm for Electromagnetic Scattering by Large Complex Objects

Jiming Song, *Member, IEEE*, Cai-Cheng Lu, *Member, IEEE*, and Weng Cho Chew, *Fellow, IEEE*

***Abstract*— The fast multipole method (FMM) and multilevel fast multipole algorithm (MLFMA) are reviewed. The number of modes required, block-diagonal preconditioner, near singularity extraction, and the choice of initial guesses are discussed to apply the MLFMA to calculating electromagnetic scattering by large complex objects. Using these techniques, we can solve the problem of electromagnetic scattering by large complex three-dimensional (3-D) objects such as an aircraft (VFY218) on a small computer.**

***Index Terms*—Electromagnetic scattering, numerical analysis.**

I. Introduction

RECENTLY, many researchers in the electromagnetics community have investigated iterative solvers for integral equations of electromagnetic scattering problems. The integral equation is discretized into a matrix equation by the method of moments (MoM). The resultant matrix equation is then solved by, for example, the conjugate gradient (CG) method, requiring $O(N^2)$ operations for the matrix-vector multiplies in each iteration, where N is the number of unknowns. A number of techniques have been proposed to speed up the evaluation of the matrix-vector multiply. The impedance matrix localization (IML) technique [1] allows the MoM matrix to be replaced by a matrix with localized clumps of large elements. The use of wavelet basis functions [2] reduces the solution time by a constant factor but not the computational complexity. The complex multipole beam approach (CMBA) [3] represents the scattered field in a series of beams produced by multipole sources located in the complex space, but it is efficient only for smooth surfaces. The multilevel matrix decomposition algorithm (MLMDA) [4] permits a fast matrix-vector multiply by decomposing the MoM matrix into a large number of blocks, each describing the interaction between distant scatterers. The multiplication of each block with a vector is executed using a multilevel scheme that resembles a fast Fourier transform (FFT).

The fast multipole method (FMM) [5]–[9] was originally proposed by Rokhlin to evaluate particle simulations and to solve static integral equation rapidly. Barnes and Hut [10] and Hernquist [11] performed n-body simulation using hierarchical method which is simpler than the FMM. But its computational complexity of $O(N \log N)$ is more than that of the FMM, which is $O(N)$ where N is the number of particles. The FMM was extended by Rokhlin to solve acoustic wave scattering problems [12] and then to solve electromagnetic scattering problems by many researchers in both two dimensions [13]–[17] and three dimensions [18]–[20]. A two-level FMM reduces both the complexity of a matrix-vector multiply and memory requirement from $O(N^2)$ to $O(N^{1.5})$ where N is the number of unknowns. A three-level FMM reduces it to $O(N^{4/3})$ [12], [21]. With a nonnested method, using the ray-propagation fast multipole algorithm (RPFMA) [16], [17], a two-level FMM reduces the complexity to $O(N^{4/3})$ also. The multilevel fast multipole algorithm (MLFMA) [22]–[25] further reduces the complexity and memory requirement. Dembart and Yip [23], [24] have implemented the MLFMA using signature function, interpolation, and filtering, with a complexity of $O(N \log^2 N)$. Song and Chew [25], implemented the MLFMA with $O(N \log N)$ complexity and memory requirement using translation, interpolation, anterpolation (adjoint interpolation), and a grid-tree data structure.

The numerical results for the radar cross section (RCS) of some simple objects like the sphere, cube, and the NASA almond are reported in [19], [20], and [25]. Since they are closed smooth objects that are not very thin, the combined field integral equation (CFIE) with uniform grids has a small condition number and converges very fast. In this paper, we will apply the MLFMA to large complex three-dimensional (3-D) objects such as an aircraft (VFY218). The number of modes required, preconditioner, near singularity extraction, and the choice of the initial guess will be discussed.

II. Multilevel Fast Multipole Algorithm (MLFMA)

To implement a multilevel fast multipole algorithm (MLFMA), we enclose the entire object in a large cube first, which is then partitioned into eight smaller cubes. Each subcube is then recursively subdivided into smaller cubes until the edge length of the finest cube is about half a wavelength. Cubes at all levels are indexed. At the finest level we find the cube in which each basis function resides by comparing the coordinates of the center of the basis function with the center of cube. We further find nonempty cubes by sorting. Only nonempty cubes are recorded using tree-structured data

Manuscript received March 19, 1996; revised June 4, 1997. This work was supported in part by the Office of Naval Research under Grant N00014-95-1-0872, by the National Science Foundation under Grant NSF ECS 93-02145, and by AFOSR under an MURI Grant.

The authors are with the Center for Computational Electromagnetics, Department of Electrical and Computer Engineering, University of Illinois, Urbana, IL 61801 USA.

Publisher Item Identifier S 0018-926X(97)07215-3.

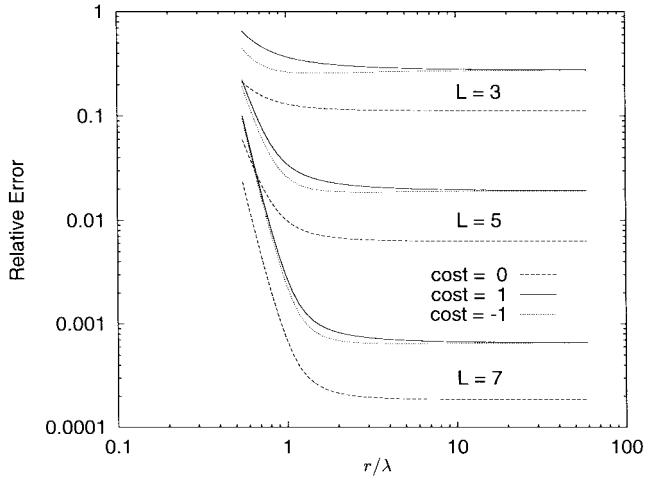

Fig. 1. Relative error in the dynamic scalar potential truncated for the first $L+1$ terms (3) as functions of the distance r/λ for $d/\lambda = 0.4$ where cost $= \hat{d} \cdot \hat{r}$.

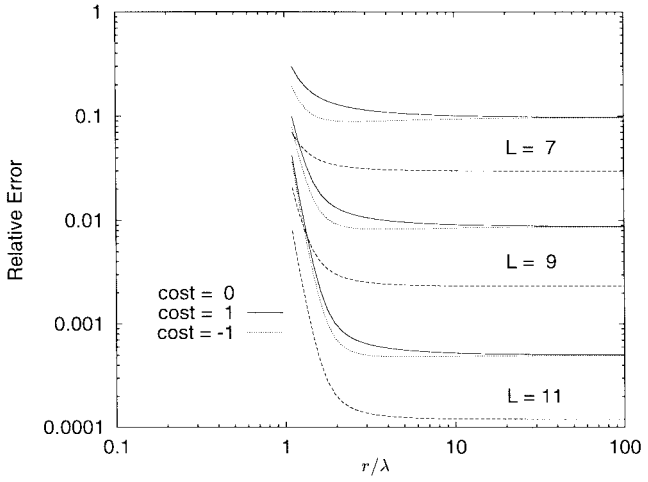

Fig. 2. Relative error in the dynamic scalar potential truncated for the first $L+1$ terms (3) as functions of the distance r/λ for $d/\lambda = 0.8$ where cost $= \hat{d} \cdot \hat{r}$.

at all levels [10], [11]. Thus, the computational cost depends only on the nonempty cubes.

A. Number of Modes

The addition theorem for 3-D dynamic scalar Green's function has the form [18], [26]

$$\frac{e^{ik|\mathbf{r}+\mathbf{d}|}}{|\mathbf{r}+\mathbf{d}|} = ik \sum_{l=0}^{\infty} (-1)^l (2l+1) j_l(kd) h_l^{(1)}(kr) P_l(\hat{d} \cdot \hat{r}) \quad (1)$$

where k is the wavenumber, j_l is a spherical Bessel function of the first kind, $h_l^{(1)}$ is a spherical Hankel function of the first kind, P_l is a Legendre polynomial, $\mathbf{r}$ and $\mathbf{d}$ are two vectors, r and d are their amplitudes with $d < r$, and $\hat{r}$ and $\hat{d}$ are their unit vectors, respectively. In this paper, $e^{-i\omega t}$ time convention is used. Using small argument approximations of j_l and $h_l^{(1)}$, we obtain the addition theorem for the 3-D static Green's function

$$\frac{1}{|\mathbf{r}+\mathbf{d}|} = \frac{1}{r} \sum_{l=0}^{\infty} (-1)^l \left(\frac{d}{r}\right)^l P_l(\hat{d} \cdot \hat{r}). \quad (2)$$

In numerical simulations, the infinite series in (1) and (2) are truncated as

$$\frac{e^{ik|\mathbf{r}+\mathbf{d}|}}{|\mathbf{r}+\mathbf{d}|} \approx ik \sum_{l=0}^{L} (-1)^l (2l+1) j_l(kd) h_l^{(1)}(kr) P_l(\hat{d} \cdot \hat{r}) \quad (3)$$

$$\frac{1}{|\mathbf{r}+\mathbf{d}|} \approx \frac{1}{r} \sum_{l=0}^{L} (-1)^l \left(\frac{d}{r}\right)^l P_l(\hat{d} \cdot \hat{r}). \quad (4)$$

For the static case, the number of modes (L) needed in (4) depends on the ratio of d to r for a given desired accuracy. This means that we can use the same number of modes for different cube sizes. Due to oscillatory nature of dynamic fields, the dynamic case is more complicated than the static case. In Figs. 1 and 2 we plot the relative error in (3) as functions of r/λ for different L and $\hat{d} \cdot \hat{r}$. Fig. 1 is for $d = 0.4\lambda$ and Fig. 2 is for $d = 0.8\lambda$. From these two figures, the accuracy does not increase even when r increases beyond $2d$. When d increases, the number of modes L required to maintain the same accuracy increases.

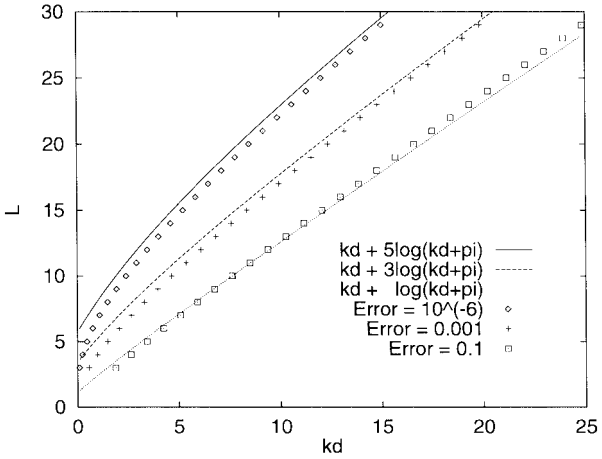

Fig. 3. Number of modes needed in (3) as functions of kd for different accuracies ($\hat{d} \cdot \hat{r} = 1$, $r/\lambda = \infty$). Some semi-empirical formulas are plotted for comparison.

In Fig. 3, we plot the number of modes L needed in (3) as functions of kd for different accuracies. Some semi-empirical formulas are plotted on the same figure for comparison. To obtain less than 0.1 relative error

$$L = kd + \ln(\pi + kd) \quad (5)$$

should be used in (3), and

$$L = kd + 5 \ln(\pi + kd) \quad (6)$$

should be used for less than 10^{-6} relative error. Equation (6) is the same as the one given in [18] for single precision. The FMM is applied to off-diagonal matrix elements only, which are two to three orders less than diagonal matrix elements for electromagnetic scattering problems. Hence, from our numerical experience, L calculated from (5) suffices for decent current solutions and RCS.

The MLFMA is used to speed up the matrix-vector multiply in the iterative methods. It decomposes the matrix-vector

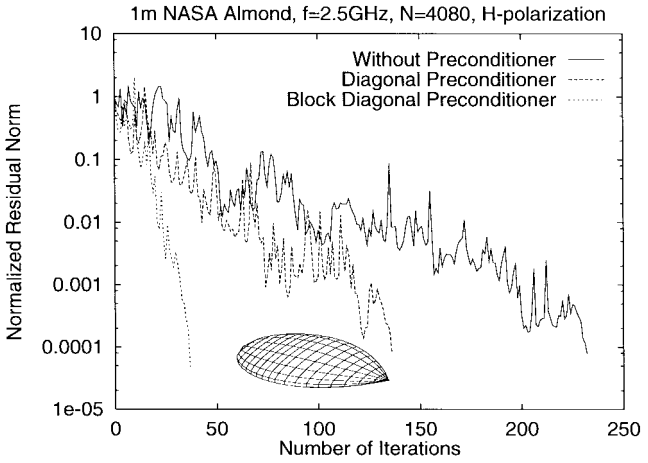

Fig. 4. Comparison of the convergence of solutions of CFIE using the biconjugate gradient (BiCG) method for a 1-m NASA almond at 2.5 GHz with or without different preconditionings.

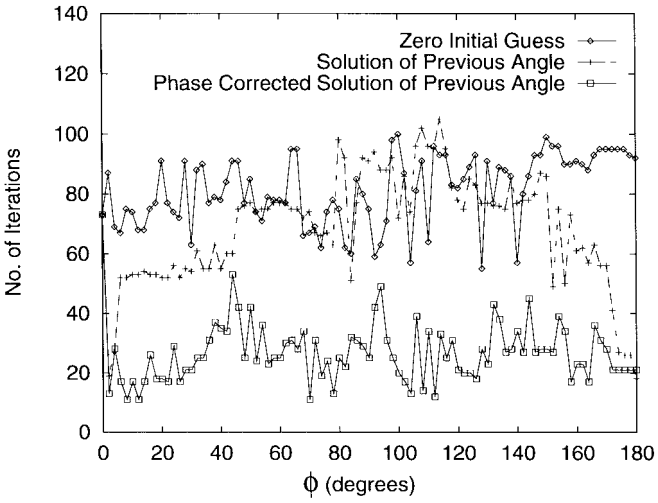

Fig. 5. Number of iterations as functions of incident angles for different initial guesses: using zero initial guess for all angles and using the solution of the previous angle as the initial guess for the next angle with/without phase corrections.

multiply into two sweeps [27]: the first sweep consists of constructing multipole expansions for each nonempty cube at all levels. Since the multipole expansions are used for calculating the fields outside the cube, they are called outer multipole expansions. As one progresses from the finest level to the coarsest level, the cube becomes larger and the number of modes required in the multipole expansions increases. To construct outer multipole expansions for each nonempty cube at all levels, the outer multipole expansions are computed at the finest level and then the expansions for larger cubes are obtained using interpolation and shifting. The second sweep consists of constructing local multipole expansions contributed from well-separated cubes at all levels. At the coarsest level, the local multipole expansions contributed from well-separated cubes are calculated using translation. At the other levels, the local expansions for smaller cubes include the contributions from parent cubes using shifting and anterpolation (adjoint interpolation) [28] and from well-separated cubes at this level but not well-separated ones at the parent level. The anterpolation matrix is the transpose of the interpolation matrix.

B. Block-Diagonal Preconditioner

The CPU time for iterative methods is proportional to the number of iterations needed to get the desired accuracy. The convergence rate depends on spectral properties of the MoM matrix. Hence, one may want to transform the original matrix equation $\overline{\mathbf{A}} \cdot \mathbf{x} = \mathbf{b}$ into $\overline{\mathbf{M}}^{-1} \cdot \overline{\mathbf{A}} \cdot \mathbf{x} = \overline{\mathbf{M}}^{-1} \cdot \mathbf{b}$ that has the same solution, but with a more favorable spectral property where $\overline{\mathbf{M}}^{-1}$ is called a preconditioner.

If basis functions in one of the finest cubes are considered as one group, the matrix $\overline{\mathbf{A}}$ has block structure and can be further divided as

$$\overline{\mathbf{A}} \cdot \mathbf{x} = (\overline{\mathbf{A}}_0 + \overline{\mathbf{A}}_1) \cdot \mathbf{x} + \overline{\mathbf{A}}_2 \cdot \mathbf{x} \tag{7}$$

where matrices $\overline{\mathbf{A}}_0$ and $\overline{\mathbf{A}}_1$ account for nearby interactions and can be derived directly from the MoM matrix and $\overline{\mathbf{A}}_0$ is the block-diagonal part. The matrix $\overline{\mathbf{A}}_2$ accounts for far interactions and $\overline{\mathbf{A}}_2 \cdot \mathbf{x}$ is performed by the MLFMA. Choosing $\overline{\mathbf{A}}_0^{-1}$ as a preconditioner, we have

$$\overline{\mathbf{A}}_0^{-1} \cdot \overline{\mathbf{A}} \cdot \mathbf{x} = \mathbf{x} + \overline{\mathbf{A}}_0^{-1} \cdot (\overline{\mathbf{A}}_1 \cdot \mathbf{x} + \overline{\mathbf{A}}_2 \cdot \mathbf{x}). \tag{8}$$

Since $\overline{\mathbf{A}}_0$ can be replaced by its LU decomposition (LUD) form for $\overline{\mathbf{A}}_0^{-1}$, the block-diagonal preconditioner needs no extra memory and no extra CPU time in each matrix-vector multiply. $\overline{\mathbf{A}}_0$ is a block-diagonal matrix with a block size of M, which is the number of unknowns in one cube. When M is a constant, the LUD of $\overline{\mathbf{A}}_0$ takes $O(M^3N/M) = O(N)$ operations. In Fig. 4, we plot the normalized residual norm as functions of iteration numbers for cases without preconditioning, diagonal preconditioning, and block-diagonal preconditioning. We find the current solution for a 1-m NASA almond at 2.5 GHz for the wave incidence on the tip. The incident electric field is parallel to its broad side. It is observed that block-diagonal preconditioning converges much faster than the other two.

C. Near-Singularity Extraction and Choice of Initial Guess

For very thin objects (like a wing), CFIE (combined field integral equation) [29] has a smaller condition number than those of an electric field integral equation (EFIE) and a magnetic field integral equation (MFIE). The null-space solutions of the EFIE will not radiate and null-space solutions of the MFIE will radiate. Therefore, both the EFIE and the MFIE cannot give correct current solutions, while the EFIE gives a correct RCS but the MFIE does not. However, the CFIE always gives a correct current solution as well as a correct RCS.

For finite-thickness objects only the self terms have a singularity and only self-singularity extraction [30] is needed. For very thin objects, both self- and near-singularity extractions [31] are required to obtain correct matrix elements.

For iterative solutions of monostatic RCS, different incident angles require different iterative solutions. Since a small change in the incident angle corresponds to a small change in the current, we use the current solution from the previous angle

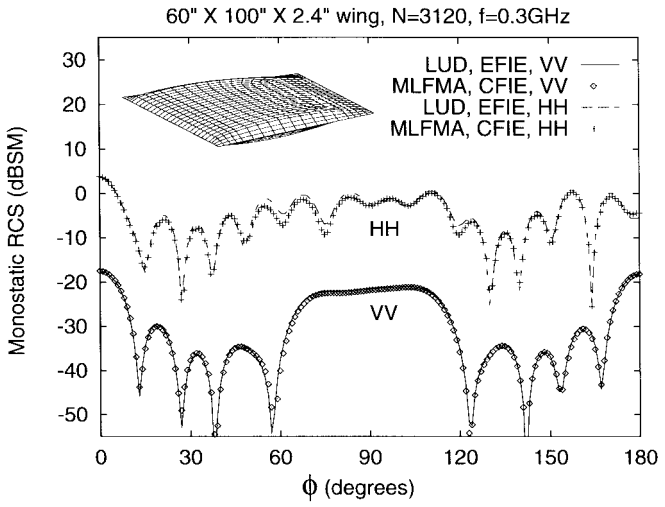

Fig. 6. Monostatic RCS of the wing (2080 flat triangular patches divided from Northrop curvilinear quad patch model) at 300 MHz as functions of ϕ in the horizontal plane.

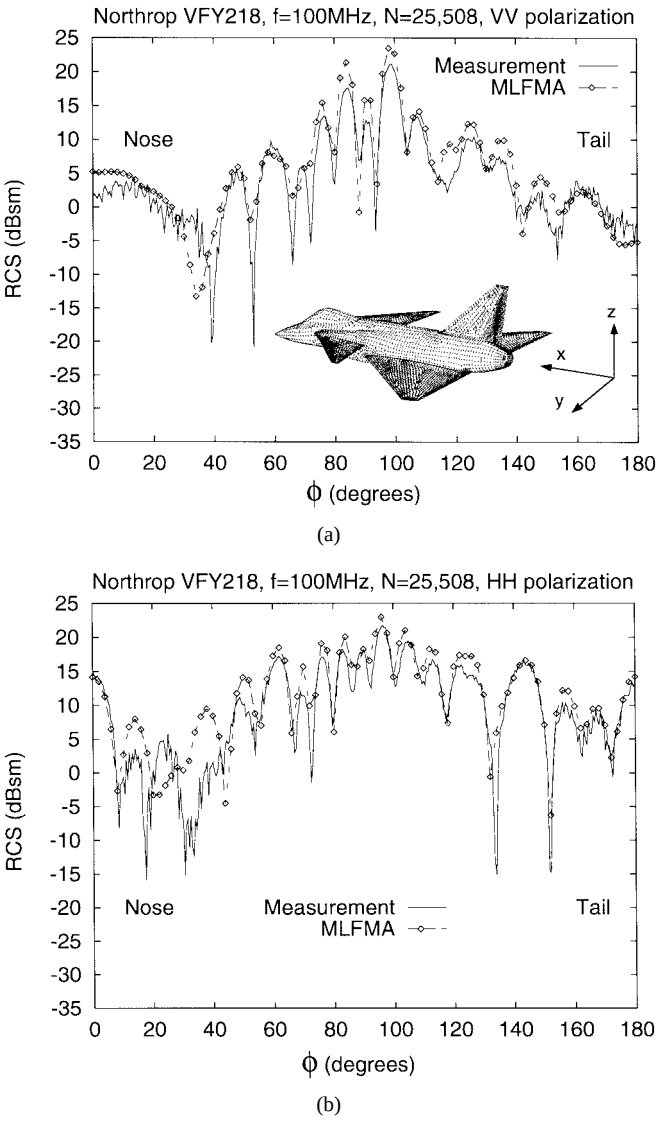

Fig. 7. Monostatic RCS of the aircraft VFY218 (Northrop curvilinear quad patch model) at 100 MHz as functions of ϕ in the horizontal plane. The measurement data are from the Naval Air Warfare Center. (a) VV polarization. (b) HH polarization.

with phase correction as the initial guess for the next angle. This technique reduces the number of iterations significantly. As an illustration, we calculate the monostatic RCS from the VFY218 at 100 MHz for vertical (VV) polarization. The VFY218 is shown in the inset of Fig. 7(a). The wings of the VFY218 are on the x-y plane (horizontal plane). Zero degree ($\phi = 0$) corresponds to the incidence angle on the nose. The VFY218 is 609 in (15.5 m) from nose to tail, 350.4 in (8.9 m) from one wing to another, and 161.4 in (4.1 m) from top to bottom. In Fig. 5, we plot the number of iterations for different incident angles using three kinds of initial guesses. The first case, which uses zero as the initial guess for all angles, needs about 85 iterations on the average for each angle. The second case, which uses the solution of the previous angle (2° step size) as the initial guess for the next angle, needs about 65 iterations per angle. The third case, which uses the phase-corrected solution of the previous angle as the initial guess for the next angle, needs only about 30 iterations per angle.

III. Numerical Results

The MLFMA has been implemented based on flat triangular patches and curvilinear quad patches using both Galerkin's method and line matching where the testing functions are constant along the line joining the centers of two adjacent patches. For curvilinear quad patches, generalized rooftop functions are used as basis functions [30]–[32]. The Rao, Wilton, and Glisson (RWG) [33] basis functions are used for flat triangular patches. The number of modes L calculated from (5) is used for numerical simulations. The code is verified by comparing the results with those in the published literature for conducting objects with different shapes like sphere, plate, cube, NASA almond, etc. Our numerical results agree very well with the analytical solutions, the measurements, and the LUD solutions. Both the memory requirements and the CPU time per iteration are of $O(N \log N)$ and a 110 592 unknown problem can be solved within 24 h on a SUN Sparc10 [25] (6 h for setup, 17 h for 29 iterations to real 0.001 normalized residual error, and 1 h for calculating 901 points of bistatic RCS).

Fig. 6 shows the monostatic RCS of a wing at 300 MHz using the LUD for the EFIE and the MLFMA for the CFIE. The wing size is 60 in $\times$ 100 in $\times$ 2.4 in and is originally modeled by Northrop using curvilinear quad patches. Dividing each quad patch as two flat triangular patches leads to a 3120 unknown problem. The wing is on the x-y plane, and zero degree ($\phi = 0$) corresponds to normal incidence to the 60 in short edge. The thickness in the z direction is only about 2% to 4% of the lengths in the x and y directions. If the near-singularity extraction is not used, we cannot obtain a correct RCS from the CFIE. Using the near-singularity extraction, we obtain a good RCS agreement between the EFIE and the CFIE. This 3120 unknown problem can also be solved using the LUD on a workstation. It is found that the RCS calculated using the MLFMA agrees very well with that using the LUD for both the EFIE and the CFIE. In Fig. 6, we plot the RCS calculated

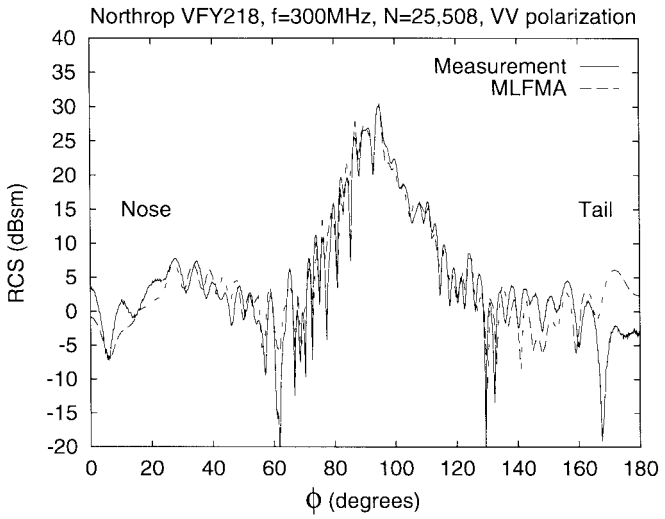

(a)

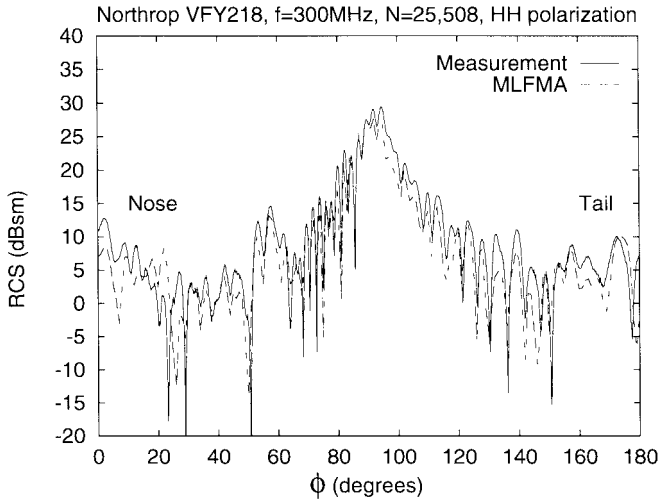

(b)

Fig. 8. Monostatic RCS of the aircraft VFY218 (Northrop curvilinear quad patch model) at 300 MHz as functions of ϕ in the horizontal plane. The measurement data are from the Naval Air Warfare Center. (a) VV polarization. (b) HH polarization.

using the LUD for the EFIE and the MLFMA for the CFIE only. Good agreement is observed between the results.

Fig. 7(a) and (b) shows the monostatic RCS for the aircraft (VFY218) at 100 MHz as functions of ϕ in the horizontal plane using the Northrop curvilinear quad patch model for horizontal (HH) and VV polarizations, respectively. Zero degree ($\phi = 0$) corresponds to an incidence angle on the nose. A five-level MLFMA is used. The measurement data are from the Naval Air Warfare Center, China Lake, CA. Good agreement between the numerical results and the measurements for both HH and VV polarizations is observed. For this 25 508 unknown problem, the MLFMA needs 167 MB of memory for this single-precision code and requires 45 h of the CPU time on one processor of an SGI Challenge machine (32 bits for each word, 25 Mflops based on the LINPACK benchmark) for 182 incident angles. In contrast, the LUD solution is estimated to need 5.2 GB of memory and 400 h of the CPU time for LUD and $O(N^2)$ calculations for each incident angle. We estimate that only for 1600 incident angles, the MLFMA would need the same CPU time as the LUD solution. But it needs memory (167 MB) much less than the LUD solution (5.2 GB). The comparison is more in favor of MLFMA when N becomes larger.

The longest edge in the Northrop VFY218 curvilinear quad patch model is 0.106λ at 100 MHz. We use the same model to predict the RCS at 300 MHz using the MLFMA. The monostatic RCS for HH and VV polarizations is shown in Fig. 8(a) and (b), respectively. The numerical results are in good agreement with the measurements.

IV. Conclusions

The MLFMA has been implemented for both flat triangular patch and curvilinear quad patch geometry descriptions to speed up the matrix-vector multiplies. Both the memory requirements and the CPU time per iteration are of $O(N \log N)$. Using a block-diagonal preconditioner, near-singularity extraction, and phase corrected previous solution for the initial guess, we can solve for the electromagnetic scattering by large complex 3-D objects such as an aircraft (VFY218) on a small computer.

Acknowledgment

The authors would like to thank M. I. Sancer and G. Antilla of Northrop for providing the geometry models of the wing and VFY218. The computer time was provided by the National Center for Supercomputing Applications (NCSA) at the University of Illinois, Urbana-Champaign. Since the submission of the manuscript for publication on March 14, 1996, the authors have solved the VFY218 at 2 GHz and problems involving 1.9 million unknowns using resources at CCEM and NCSA.

References

[1] F. X. Canning, "Solution of IML form of moment method problems in 5 iterations," *Radio Sci.*, vol. 30, no. 5, pp. 1371–1384, Sept./Oct. 1995.
[2] R. L. Wagner and W. C. Chew, "A study of wavelets for the solution of electromagnetic integral equations," *IEEE Trans. Antennas Propagat.*, vol. 43, pp. 802–810, Aug. 1995.
[3] A. Boag and R. Mittra, "Complex multipole beam approach to electromagnetic scattering problems," *IEEE Trans. Antennas Propagat.*, vol. 42, pp. 366–372, Mar. 1994.
[4] E. Michielssen and A. Boag, "Multilevel evaluation of electromagnetic fields for the rapid solution of scattering problems," *Microwave Opt. Technol. Lett.*, vol. 7, no. 17, pp. 790–795, Dec. 5, 1994.
[5] V. Rokhlin, "Rapid solution of integral equations of classical potential theory," *J. Comput. Phys.*, vol. 60, no. 2, pp. 187–207, Sept. 15, 1985.
[6] L. Greengard and V. Rokhlin, "A fast algorithm for particle simulations," *J. Comput. Phys.*, vol. 73, pp. 325–348, Dec. 1987.
[7] ——, "Fast methods in the three dimensions," in *Vortex Methods*, C. Anderson and C. Greengard, Eds. Berlin, Germany: Springer-Verlag, 1988, lecture notes in Mathem., 1360.
[8] J. Carrier, L. Greengard, and V. Rokhlin, "A fast adaptive multipole algorithm for particle simulations," *SIAM J. Sci. Stat. Comput.*, vol. 9, pp. 669–686, July 1988.
[9] J. Ambrosiano, L. Greengard, and V. Rokhlin, "The fast multipole method for gridless particle simulation," *Comput. Phys. Commun.*, vol. 48, pp. 117–125, 1988.
[10] J. Barnes and P. Hut, "A hierarchical $O(N \log N)$ force calculation algorithm," *Nature*, vol. 324, pp. 446–449, Dec. 1986.
[11] L. Hernquist, "Hierarchical N-body methods," *Comput. Phys. Commun.*, vol. 48, pp. 107–115, 1988.

[12] V. Rokhlin, "Rapid solution of integral equations of scattering theory in two dimensions," *J. Comput. Phys.*, vol. 36, no. 2, pp. 414–439, Feb. 1990.
[13] N. Engheta, W. D. Murphy, V. Rokhlin, and M. S. Vassiliou, "The fast multipole method (FMM) for electromagnetic scattering problems," *IEEE Trans. Antennas Propagat.*, vol. 40, pp. 634–641, June 1992.
[14] L. R. Hamilton, M. A. Stalzer, R. S. Turley, J. L. Visher, and S. M. Wandzura, "Scattering computation using the fast multipole method," in *IEEE APS Int. Symp. Dig.*, Ann Arbor, MI, June 1993, pp. 852–855.
[15] C. C. Lu and W. C. Chew, "Fast algorithm for solving hybrid integral equations," *Proc. Inst. Elect. Eng.*, vol. 140, pt. H, no. 6, pp. 455–460, Dec. 1993.
[16] R. Coifman, V. Rokhlin, and S. Wandzura, "Faster single-stage multipole method for the wave equation," in *10th Annu. Rev. Progress Appl. Computat. Electromagn.*, Monterey, CA, Mar. 1994, pp. 19–24.
[17] R. L. Wagner and W. C. Chew, "A ray-propagation fast multipole algorithm," *Microwave Opt. Technol. Lett.*, vol. 7, no. 10, pp. 435–438, July 1994.
[18] R. Coifman, V. Rokhlin, and S. Wandzura, "The fast multipole method for the wave equation: A pedestrian prescription," *IEEE Antennas Propagat. Mag.*, vol. 35, pp. 7–12, June 1993.
[19] J. M. Song and W. C. Chew, "Fast multipole method solution using parametric geometry," *Microwave Opt. Technol. Lett.*, vol. 7, no. 16, pp. 760–765, Nov. 1994.
[20] ———, "Fast multipole method solution of the combined field integral equation," in *11th Annu. Rev. Progress Appl. Computat. Electromagn.*, Monterey, CA, Mar. 1995, pp. 629–636.
[21] V. Rokhlin, "Diagonal forms of translation operators for the Helmholtz equation," *Appl. Computat. Harmon. Analysis*, vol. 1, pp. 82–93, 1993.
[22] C. C. Lu and W. C. Chew, "A multilevel algorithm for solving boundary integral equations of wave scattering," *Microwave Opt. Technol. Lett.*, vol. 7, no. 10, pp. 466–470, July 1994.
[23] B. Dembart and E. Yip, "A 3-D fast multipole method for electromagnetics with multiple levels," in *11th Annu. Rev. Progress Appl. Computat. Electromagn.*, Monterey, CA, Mar. 1995, pp. 621–628.
[24] M. A. Epton and B. Dembart, "Multipole translation theory for the three-dimensional Laplace and Helmholtz equations," *SIAM J. Sci. Comput.*, vol. 16, no. 4, pp. 865–897, July 1995.
[25] J. M. Song and W. C. Chew, "Multilevel fast-multipole algorithm for solving combined field integral equations of electromagnetic scattering," *Microwave Opt. Technol. Lett.*, vol. 10, no. 1, pp. 14–19, Sept. 1995.
[26] M. Abramowitz and I. A. Stegun, *Handbook of Mathematical Functions*. New York: Dover, 1965.
[27] C. R. Anderson, "An implementation of the fast multipole method without multipoles," *SIAM J. Sci. Stat. Comput.*, vol. 13, no. 4, pp. 923–947, Apr. 1992.
[28] A. Brandt, "Multilevel computations of integral transforms and particle interactions with oscillatory kernels," *Comput. Phys. Commun.*, vol. 65, pp. 24–38, 1991.
[29] J. R. Mautz and R. F. Harrington, "H-field, E-field, and combined-field solutions for conducting bodies of revolution," *Archiv für Elektronik Übertragung* vol. 32, pp. 157–163, 1978.
[30] J. M. Song and W. C. Chew, "Moment method solutions using parametric geometry," *J. Electromagn. Waves and Appl.*, vol. 9, nos. 1/2, pp. 71–83, 1995.
[31] G. Antilla, Y. C. Ma, P. V. Alstine, and M. I. Sancer, "Hybrid finite element-method of moments for electromagnetic prediction of complex 3-D geometries," in *Course Note, IEEE AP-S Int. Symp. URSI Radio Sci. Meet.*, Newport Beach, CA, June 1995.
[32] G. E. Antilla and N. G. Alexopoulos, "Scattering from complex three-dimensional geometries using a curvilinear hybrid finite-element-integral equation approach," *J. Opt. Soc. Amer. A*, vol. 11, no. 4, pp. 1445–1457, Apr. 1994.
[33] S. M. Rao, D. R. Wilton, and A. W. Glisson, "Electromagnetic scattering by surfaces of arbitrary shape," *IEEE Trans. Antennas Propagat.*, vol. AP-30, pp. 409–418, May 1982.

Jiming Song (S'92–M'95), for photograph and biography, see p. 245 of the February 1997 issue of this TRANSACTIONS.

Cai-Cheng Lu (S'93–M'95), for photograph and biography, see p. 543 of the March 1997 issue of this TRANSACTIONS.

Weng Cho Chew (S'79–M'80–SM'86–F'93), for photograph and biography, see p. 245 of the February 1997 issue of this TRANSACTIONS.